


Article

# Photocatalytic and Pozzolanic Properties of Nano-SiO<sub>2</sub>/Al<sub>2</sub>O<sub>3</sub>-TiO<sub>2</sub> Powder for Functional Mortar

Jong-Won Lee <sup>1</sup>, Young-Il Jang <sup>2,\*</sup>, Wan-Shin Park <sup>2</sup>, Sun-Woo Kim <sup>2</sup> and Byung-Jae Lee <sup>3</sup>

<sup>1</sup> Department of Convergence Systems Engineering, Chungnam National University, 99 Daehak-ro Yuseong-gu, Daejeon 34134, Korea; asca28@cnu.ac.kr

<sup>2</sup> Department of Construction Engineering Education, Chungnam National University, 99 Daehak-ro Yuseong-gu, Daejeon 34134, Korea; salshin@cnu.ac.kr (W.-S.P.); sw.kim@cnu.ac.kr (S.-W.K.)

<sup>3</sup> Department of Civil Engineering, Daejeon University, 62 Daehak-ro Dong-gu, Daejeon 34520, Korea; bjlee@dju.kr

\* Correspondence: jang1001@cnu.ac.kr; Tel.: +82-42-821-8582

Received: 24 January 2019; Accepted: 23 March 2019; Published: 28 March 2019



**Abstract:** The present study intended to find a way to use TiO<sub>2</sub>, one of the most widely used photocatalysts, as a construction material. To that end, nano-SiO<sub>2</sub>/Al<sub>2</sub>O<sub>3</sub>-TiO<sub>2</sub> powder (NTCP) was synthesized by coating SiO<sub>2</sub> and Al<sub>2</sub>O<sub>3</sub> support materials with TiO<sub>2</sub>. The NTCP was anatase phase spherical particles, specific surface areas were 319 m<sup>2</sup>/g and 267 m<sup>2</sup>/g for the SiO<sub>2</sub>-TiO<sub>2</sub> powder and Al<sub>2</sub>O<sub>3</sub>-TiO<sub>2</sub> powder. UV absorption test results showed the developed NTCP had a light absorption peak at wavelengths of 380 nm or below, and its absorbance was much larger than that of commercial TiO<sub>2</sub>. The NTCP formed smaller pores on the surface than commercial TiO<sub>2</sub>. As a result, the flow of the mortar decreased as the adsorption strength increased and combined a large number of water molecules. In addition, the Pozzolanic reaction by SiO<sub>2</sub> and Al<sub>2</sub>O<sub>3</sub> used as support materials produced many calcium silicate hydrate (C-S-H) and calcium aluminate hydrate (C-A-H). This has shown an increased strength of mortar mixed with the NTCP by promoting a nucleation effect and reducing the filling effect and the number of harmful holes in the mortar.

**Keywords:** construction material; nano-TiO<sub>2</sub>; mortar; compress strength; micro structure

## 1. Introduction

With rapid industrial development, the air pollution caused by factories fumes, SO<sub>x</sub>, exhaust emissions, and fine dust has been continuously increasing. Accordingly, environmental problems such as global warming have recently emerged as global issues of concern [1,2]. Vehicles are on-road mobile pollution sources, while industrial boilers and power generation facilities are major stationary pollution sources. Notably, NO<sub>x</sub>, a harmful air pollutant, comes from both pollution source types. Currently, NO<sub>x</sub> pollution produced by motor vehicle emissions have reached alarming levels in major cities, causing respiratory disease, photochemical smog, and acid rain [3]. Accordingly, there is increasing social demand for measures to reduce air pollution, and in particular, pollution caused by NO<sub>x</sub> including NO and NO<sub>2</sub> from on-road mobile sources.

Measures for reducing NO<sub>x</sub> air pollution include the purification and detoxification of NO<sub>x</sub> via photocatalytic reactions. The method is based on the principle that a photocatalyst, while reacting with sunlight, tends to absorb air pollutants such as NO<sub>x</sub> and organic chlorine compounds [4–7].

The photocatalyst used for that purpose must have excellent optical activity, high absorbance of visible light and ultraviolet light, an optimal energy range suitable for reactions, biological and chemical inertness, optical stability, low cost, and more. Among all other candidates, TiO<sub>2</sub> is known

to be the most effective.  $\text{TiO}_2$  is superior to other photocatalysts, in particular, its chemical stability, and is not eroded by most acids, bases, or organic solvents. Due to these features, it is widely used in construction [8–12].

In the construction field, researchers have attempted to find methods of applying photo catalysts to self-cleaning structures, and to develop photocatalytic concrete for road pavement construction and paving blocks to reduce on-road mobile pollution caused by cars [13–16]. Since the mid-2000s, researchers mainly from Japan, Italy, Belgium, the US, and China have been engaged in research and development of concrete pavement construction and self-cleaning technologies using photocatalytic materials such as  $\text{TiO}_2$  [17,18]. When concrete pavement using  $\text{TiO}_2$  is illuminated by sunlight, the  $\text{TiO}_2$  on the surface reacts with the light and decomposes  $\text{NO}_x$  into  $\text{NO}_3^-$  via photocatalytic reactions. Subsequently, the byproducts are washed away when it rains in  $\text{HNO}_3$  aqueous solution form. As a result, the concentration of  $\text{NO}_x$  in the atmosphere is reduced. Additionally,  $\text{NO}_3^-$  can be eliminated when it reaches a groundwater basin via biological denitrifying oxidation. The method is likewise based on complex reaction mechanisms [19,20].

Based on these principles, mortar and concrete mixed with  $\text{TiO}_2$  are widely used for self-cleaning, deodorization, and air purification purposes, e.g., in road pavement, and in buildings, stadiums, and theaters as precast exterior materials. In the civil sector, road pavement and paving blocks which serve as public infrastructure have a higher ratio of surface area to volume than most other structures and, hence, they have an advantage in that they can maximize photocatalytic efficiency [3].

In the above cases where  $\text{TiO}_2$  was applied to structures, the construction was conducted using cement, part of which was replaced with  $\text{TiO}_2$ . This partial replacement method, however, consumes a greater quantity of  $\text{TiO}_2$ , and hinders the hydration reaction of cement, thus degrading the concrete's strength [21]. Also, the  $\text{TiO}_2$  inside the concrete is never exposed to light sources or exhaust gases, so it is unable to trigger a photocatalytic reaction [22,23].

To overcome these problems, there has been extensive research on the use of new composite materials. Han et al. [24] coated nano- $\text{TiO}_2$  with  $\text{SiO}_2$ , and, as a result, the  $\text{SiO}_2$ -coated nano- $\text{TiO}_2$  exhibited improved dispersibility in water and a binder due to increased negative charges. The researchers applied the material to a designed mix of reactive powder concrete (RPC) to improve its mechanical properties. However, they focused more on strength enhancement by the filler effect than on the functionality of the  $\text{TiO}_2$ . In contrast, Kummaruddin and Stephan [25] conducted research on the photocatalytic activity of sand and silica fume coated with  $\text{TiO}_2$  via the sol-gel process. They reported that the developed  $\text{TiO}_2$  coated sand and silica fume efficiently decomposed  $\text{NO}_x$  and, thus, could be used as a photocatalytic material for the external walls of air purifying buildings.

Likewise, previous research [26–30] has focused on either exploring the photocatalytic characteristics of commercial  $\text{TiO}_2$  or improving the mechanical properties of concrete, but not in parallel. Unfortunately, little attention has been paid to the development of  $\text{TiO}_2$  materials that can serve as more effective photocatalysts when mixed into mortar without significantly degrading the strength of mortar and concrete.

This study is a basic step to develop functional mortar that can purify air pollution using  $\text{TiO}_2$ , so in order to develop functional  $\text{TiO}_2$ , we fabricated Nano- $\text{SiO}_2/\text{Al}_2\text{O}_3\text{-TiO}_2$  powder (NTCP) coated with  $\text{TiO}_2$  by using  $\text{SiO}_2$  and  $\text{Al}_2\text{O}_3$  as supports and evaluated the performance. In addition, we fabricated mortar which can be applied to the shotcrete and surface of concrete secondary products with the NTCP, and analyzed the reaction to cement and the mechanical performance.

## 2. Materials and Methods

### 2.1. Materials

#### 2.1.1. Nano- $\text{SiO}_2/\text{Al}_2\text{O}_3\text{-TiO}_2$ Powder (NTCP)

This study aims at finding optimal coating conditions by analyzing the efficiency and characteristics of surface coating methods through depositions, such as chemical vapor deposition

(CVD), sol-gel, and atomic layer deposition (ALD), to derive the optimal coating method for producing NTCP. Results of the test showed that the Sol-gel method could maintain uniform status compared to CVD and ALD, and there were no deformations, making it possible to obtain highly pure and highly homogenous powders. It was also found that sol-gel method is the most superior in terms of economic feasibility when utilizing it as construction materials in future.

NTCP was developed via the sol-gel method using TTIP (Titanium isopropoxide;  $Ti(OC_3H_7)_4$ ) as a precursor for  $TiO_2$ , and TEOS (tetraethy-lorthosilicate;  $Si(OC_2H_5)_4$ ) and ALP (aluminum isopropoxide;  $Al(OCH_2(CH_3)_2)_3$ ) as the precursors for  $SiO_2$  and  $Al_2O_3$ , respectively. Nitric acid and acetic acid were used as catalysts, and ethanol and iso-propanol were used as solvents. To determine the specific surface area of the NTCP that would be suitable for construction applications, various mix designs were developed, as shown in Table 1. The developed NTCP were heat treated at temperatures ranging from 400 to 800 °C for crystallographic analysis. Reagents used in testing are listed in Table 2. Figure 1 describes the synthesis method for the Nano- $SiO_2$ - $TiO_2$  powder used in the present study.

**Table 1.** Composition of nano  $SiO_2$ - $TiO_2$  powder and  $Al_2O_3$ - $TiO_2$  powder.

Mix ID	$TiO_2$ (Mol)	$SiO_2$ (Mol)	$Al_2O_3$ (Mol)
ST-1	0.9	0.1	-
ST-2	0.7	0.3	-
ST-3	0.5	0.5	-
AT-1	0.9	-	0.1
AT-2	0.7	-	0.3
AT-3	0.5	-	0.5

**Table 2.** Physical properties of materials.

Starting Materials	Chemical Formula	Formula Weight	Density (g/mL)	Grade
TTIP (Titanium isopropoxide)	$Ti(OC_3H_7)_4$	284.26	0.963	Purity = 97%
TEOS (Tetraethy lorthosilicate)	$Si(OC_2H_5)_4$	208.30	0.934	Purity = 98%
ALP (Aluminum isopropoxide)	$Al(OCH_2CH_3)_2$	204.24	1.035	Purity = 98%

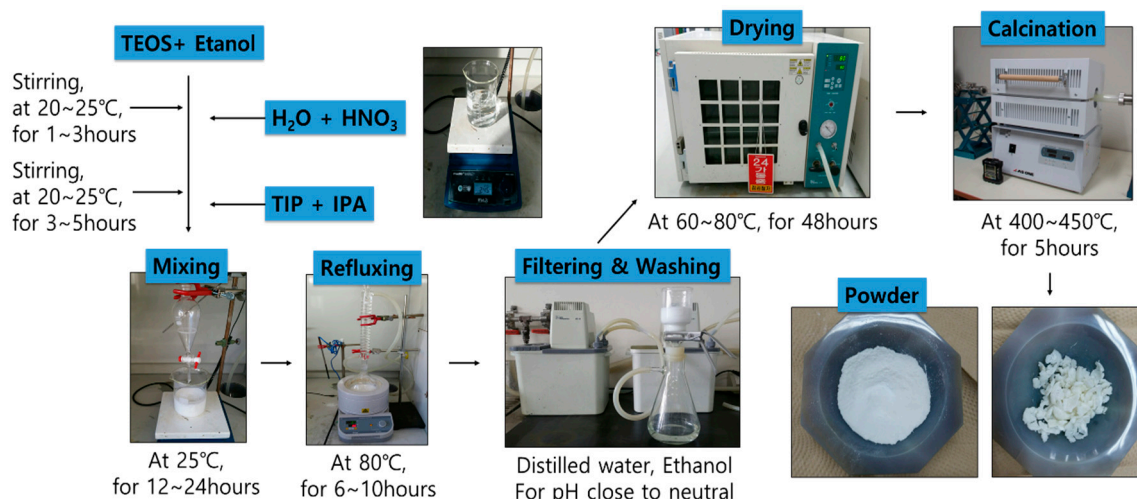


**Figure 1.** Production process of NTCP.

### 2.1.2. Commercial $TiO_2$

The commercial  $TiO_2$  used as the comparative of the NTCP prepared in this study is the nano- $TiO_2$  of P company. The physical and chemical properties of the commercial  $TiO_2$  used are presented in Table 3.

**Table 3.** Physical properties of commercial TiO<sub>2</sub>.

Purity (TiO <sub>2</sub> )	Fe <sub>2</sub> O <sub>3</sub>	H <sub>2</sub> O	Particle Size	pH	Ignition Loss
98.0%	0.008%	0.4%	250–350 nm	7.0–8.0	0.3%

### 2.1.3. Cement

The cement used for this study is Ordinary Portland Cement (OPC) which has density is 3.14 g/cm<sup>3</sup>, Blaine fineness is 3492 cm<sup>2</sup>/g. The physical and chemical properties of OPC are as shown in Table 4.

**Table 4.** Physical and chemical properties of OPC.

Density (g/cm <sup>3</sup> )	Blaine Fineness (cm <sup>2</sup> /g)	Chemical Properties (%)						
		SiO <sub>2</sub>	Al <sub>2</sub> O <sub>3</sub>	Fe <sub>2</sub> O <sub>3</sub>	CaO	MgO	SO <sub>3</sub>	Ignition Loss
3.14	3492	21.1	4.65	3.14	62.8	2.81	2.1	2.18

### 2.1.4. ISO Graded Standard Sand

The sand was rounded particles and content of silicon dioxide was 98% or more, and the particle size was in accordance with the specification of KS L ISO 679 Methods of testing cements-Determination of Strength. The particle size distribution of ISO graded standard sand are as shown in Table 5.

**Table 5.** Particle size distribution of ISO graded standard sand.

Sieve Size(mm)	2.0	1.6	1.0	0.5	0.16	0.08
Accumulated charge in the sieve (%)	0	7 ± 5	33 ± 5	67 ± 5	87 ± 5	99 ± 5

## 2.2. Experiment Method of NTCP

### 2.2.1. BET

The Brunauer–Emmett–Teller (BET) method was used to determine the specific surface area, presence and size of pores, and the pore volume of a given specimen. Specific surface area is one of the most important factors determining photocatalytic efficiency. To assess the effect of the SiO<sub>2</sub> and Al<sub>2</sub>O<sub>3</sub> addition on the specific surface area of a given specimen, the specific surface area was measured for both a commercial TiO<sub>2</sub> specimen and the nano-TiO<sub>2</sub> developed in the present study. BET surface analysis was performed using the Micrometrics ASAP 2010 system (Micrometrics, Norcross, GA, USA) in which specimens were heat treated at 200 °C for 4 h, and nitrogen absorbance was measured for the specimens at −196 °C.

### 2.2.2. XRD

Generally, TiO<sub>2</sub> produced via the sol-gel method tends to be amorphous, but when it is heat treated, a phase transition occurs from amorphous to anatase and rutile phases. X-ray powder diffraction (XRD) analysis was conducted to confirm the occurrence of such phase transitions and their effect on phase transitions of the SiO<sub>2</sub> and Al<sub>2</sub>O<sub>3</sub>.

The X-ray diffraction analysis was conducted using D8 Advance diffractometer (Bruker-AXS, Shibuya, Tokyo, Japan) attached with a Lynx Eye position sensitive detector and Cu target. The diffraction pattern was obtained in the conditions of 5° to 95° 2θ sectors, 0.01° step size, and 1 sec per step, and 0.3° divergence slit and 2.5° secondary Soller slit were used. In order to obtain qualitative analysis of specimens and fundamental parameters for device elements, X-ray diffraction patterns were obtained for the original specimen and standard specimen (LaB6, SRM 660b, NIST, Gaithersburg, MD, USA) under the same conditions.



### 2.2.3. SEM

Morphology of the NTCP was examined using a scanning electron microscope (SEM, Akishima, Tokyo, Japan) with voltages between 10–30 kV and a secondary electron detector. In combination, an energy dispersive X-ray spectroscope (EDS, Akishima, Tokyo, Japan) was used to obtain the elemental composition of the particle surface.

### 2.2.4. TEM

The morphology of NTCP was assessed by transmission (TEM) electron microscopy, coupled with for these analyses a Quanta Inspect F scanning electron microscope (1.2 nm resolution, Hillsboro, OR, USA) with EDX and a Tecnai TM G<sup>2</sup> F30 S-TWIN high-resolution transmission electron microscope (HR-TEM, Hillsboro, OR, USA) equipped with STEM—HAADF detector (Hillsboro, OR, USA), EDX, and EELS were used.

### 2.2.5. UV-Vis

UV–VIS analysis was employed to evaluate the absorption rate of the developed NTCP in visible light, using a UV–VIS Spectrophotometer Solid Spec S-3100 of SCINCO (Gangnam, Seoul, Korea). The absorbance of the visible light photocatalysts was measured at wavelength ranges between 300 and 700 nm.

## 2.3. Mix Proportion and Preparation of Mortar Test Specimens

### 2.3.1. Mix Proportion

The mortar mix proportion had a binder to sand ratio of 1:3 and W/B = 50% in accordance with International Organization for Standardization (ISO) 679 Methods of testing cements determination of strength. To analyze the effect of NTCP on the hydration reaction of concrete, the amount of added NTCP was adjusted according to the replacement ratio of cement, and the resulting mix designs are shown in Table 6.

**Table 6.** Mix proportion.

Test ID	W/B (%)	Mix Composition (g)				
		Sand	Water	Cement	Powder	
Plain				450	-	
TiO <sub>2</sub>	2%			441	9	
	4%			432	18	
	6%			423	27	
	8%			414	36	
	10%			405	45	
SiO <sub>2</sub> /TiO <sub>2</sub>	2%	50	1350	225	441	9
	4%				432	18
	6%				423	27
	8%				414	36
	10%				405	45
Al <sub>2</sub> O <sub>3</sub> /TiO <sub>2</sub>	2%			441	9	
	4%			432	18	
	6%			423	27	
	8%			414	36	
	10%			405	45	

### 2.3.2. Preparation of Test Specimens

To measure mortar compressive strength, test specimens of 40 mm × 40 mm × 160 mm were prepared according to ISO 679. After curing for 24 h in a constant temperature and moisture room, the mortar underwent removal of form followed by water curing at 20 °C. Compressive strength was measured for test specimens at varying ages.

### 2.3.3. Mortar Test Method

The flow test was conducted after mixing of mortar in accordance with American Society for Testing and Materials (ASTM) Standards: C 1437 Standard Test Method for Flow of Hydraulic Cement Mortar. The flexural strengths and compressive strength tests were performed according to ISO 679, and measurements were taken at age 3, 7 and 28 days. A universal testing machine (UTM) of 100 ton was used to measure the compressive strength by age.

## 3. Experiment Results and Analysis

### 3.1. BET Analysis

The BET results for different precursor mixing ratios are shown in Table 7. When the ratio was 0.3 mol, both SiO<sub>2</sub> and Al<sub>2</sub>O<sub>3</sub> had a maximum specific surface area of 319 m<sup>2</sup>/g and 267 m<sup>2</sup>/g, respectively. These values tended to decrease when the ratio exceeded 0.5 mol. This phenomenon is ascribed to the varying solubility of alkoxide in the solvents at different mixing ratios. Namely, as the average particle size of NTCP increases, the relative specific surface area decreases.

Since the specific surface area is an important determining factor for photocatalytic efficiency, ST-2 and AT-2 mixing ratios, which exhibited the largest specific surface area, were considered to be the most suitable construction materials. Additionally, crystalline properties were studied while changing heat treatment temperature and thus crystal size.

The results showed that as the heat treatment temperature increased, the specific surface area decreased, and this was due to the enhanced crystal growth at increased temperatures, as well as the fact that the specific surface area of TiO<sub>2</sub> is relatively smaller than that of SiO<sub>2</sub> and Al<sub>2</sub>O<sub>3</sub>. At heat treatment temperatures of 700 °C and above sintering occurred, leading to a sudden decrease in specific surface area.

As a result, the optimal mix design for NTCP for construction purposes considering photocatalytic efficiency—was determined to be the mixture of 0.7 mol Ti and 0.3 mol precursor, heat treated at 450 °C. This combination exhibited the largest specific surface area.

**Table 7.** Result of BET.

Powder	Surface Area (m <sup>2</sup> /g)	Pore Volume (cm <sup>3</sup> /g)	Pore Size (Å)
TiO <sub>2</sub>	8.5	0.01	82
SiO <sub>2</sub> -TiO <sub>2</sub>	ST-1	121	0.27
	ST-2	319	0.39
	ST-3	241	0.31
Al <sub>2</sub> O <sub>3</sub> -TiO <sub>2</sub>	AT-1	112	0.26
	AT-2	267	0.33
	AT-3	149	0.29

### 3.2. XRD Analysis

XRD analysis was performed both on commercial TiO<sub>2</sub> and the NTCP produced using the optimal mixing ratio, and the analytical results are shown in Figure 2. TiO<sub>2</sub> is classified according to crystal structure, as follows: anatase phase with excellent photodecomposition activity, rutile phase with excellent thermal stability, and brookite phase only found in minerals. The reference peaks for the

anatase phase are peaks at  $2\theta = 25.302(101)$ ,  $38.608(112)$ ,  $48.091(200)$ ,  $48.103(200)$ ; those for rutile phase are peaks at  $2\theta = 27.461(110)$ ,  $36.116(101)$ ,  $39.311(200)$ ; and those for brookite phase are peaks at  $2\theta = 42.375(221)$ ,  $52.057(240)$ ,  $57.736(232)$ ,  $54.581(311)$ . XRD analytical results confirmed that the NTCP developed in the present study had only anatase phase. No rutile or brookite phase peaks were observed. This phenomenon is ascribed to the fact that the more thermally stable  $\text{SiO}_2$  and  $\text{Al}_2\text{O}_3$  effectively suppressed the phase transition of the  $\text{TiO}_2$ .

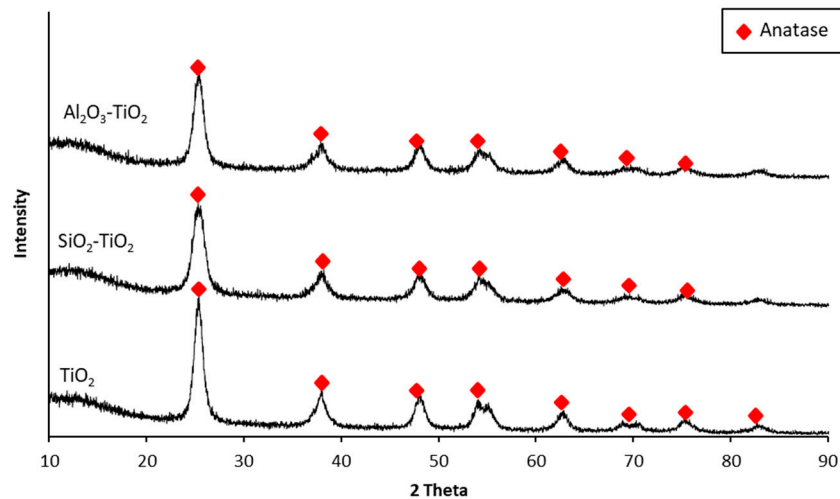


Figure 2. XRD pattern of commercial  $\text{TiO}_2$  and NTCP.

### 3.3. SEM Analysis

When SEM images of commercial  $\text{TiO}_2$  and the NTCP are shown in Figures 3 and 4. In the commercial  $\text{TiO}_2$ , the particle size was larger, and aggregation spots were more frequently observed. In contrast, neither aggregation spots nor single phases of  $\text{TiO}_2$ ,  $\text{SiO}_2$ , and  $\text{Al}_2\text{O}_3$  were observed in the NTCP developed in the present study. Also, no peaks were found for the  $\text{Al}_2\text{TiO}_5$  phase, a compound of  $\text{TiO}_2$  and  $\text{Al}_2\text{O}_3$ , confirming that the NTCP had been successfully synthesized. In line with the XRD results, the NTCP was found to be anatase phase spherical particles, and no linear shaped particles of the rutile phase were observed.

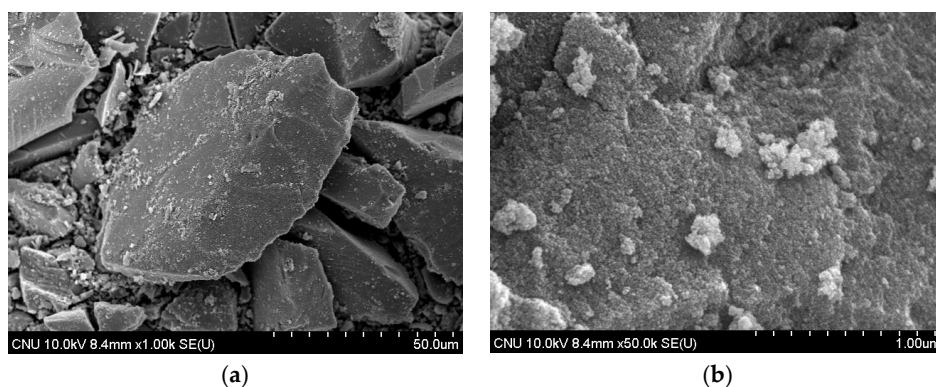
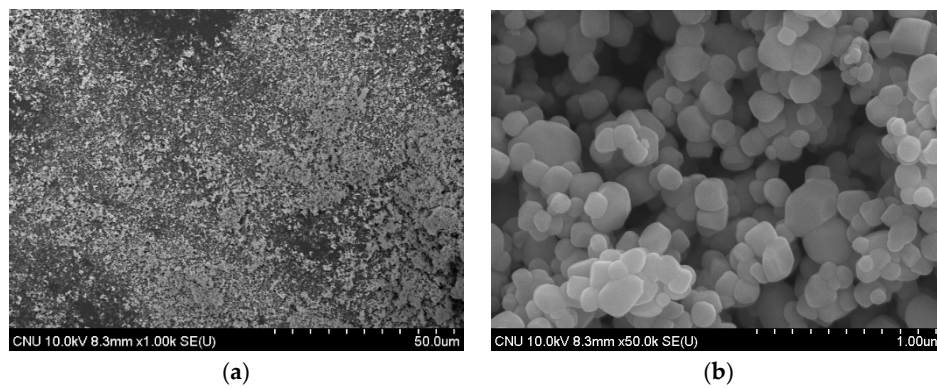


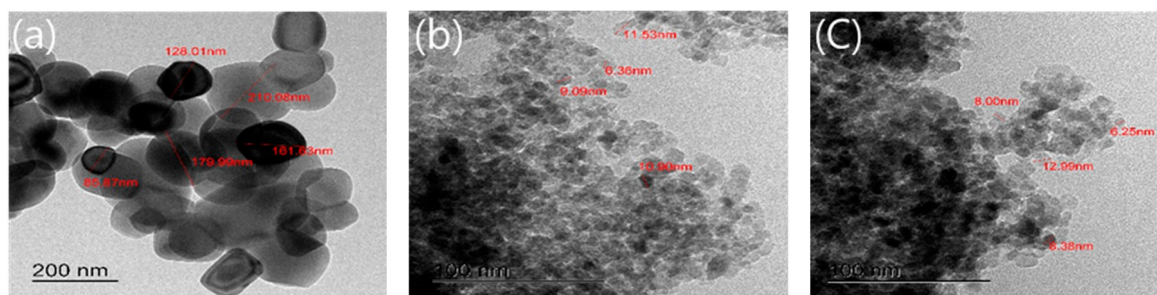
Figure 3. SEM image of commercial  $\text{TiO}_2$ , (a) commercial  $\text{TiO}_2$  (1000 $\times$ ); and (b) commercial  $\text{TiO}_2$  (50,000 $\times$ ).



**Figure 4.** SEM image of NTCP, (a) NTCP (1000 $\times$ ); and (b) NTCP (50,000 $\times$ )

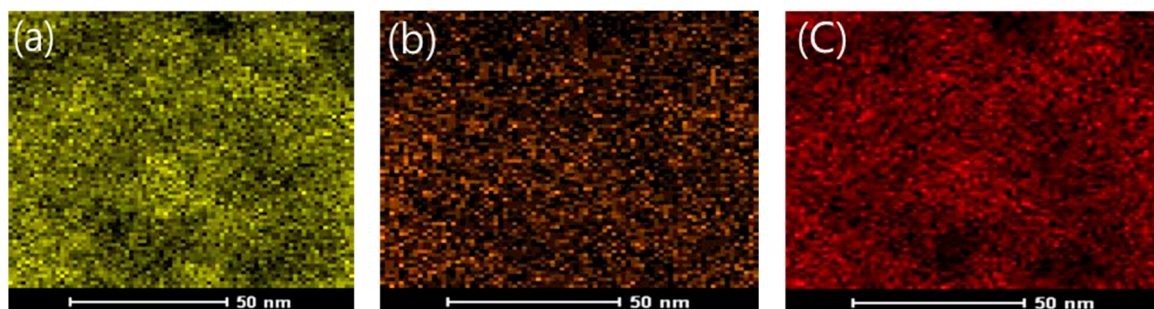
### 3.4. TEM Analysis

Figure 5 shows the results of TEM observation of the commercial  $\text{TiO}_2$  and the NTCP. Here, the particle size and shape of both specimens were compared. For commercial  $\text{TiO}_2$ , the particle size was not uniform, varying from 85.87 to 210.08 nm. In contrast, for the NTCP, the particle size of the  $\text{SiO}_2$ - $\text{TiO}_2$  powder ranged between 6.36 and 11.53 nm, and the particle size of the  $\text{Al}_2\text{O}_3$ - $\text{TiO}_2$  powder ranged between 6.25 and 12.99 nm. This means that the NTCP has a relatively more uniform particle size than commercial  $\text{TiO}_2$ .



**Figure 5.** TEM image of commercial  $\text{TiO}_2$  and NTCP (a) commercial  $\text{TiO}_2$  (b)  $\text{SiO}_2$ - $\text{TiO}_2$ , and (c)  $\text{Al}_2\text{O}_3$ - $\text{TiO}_2$ .

EDX analysis was carried out to visualize the structure of the NTCP's coating layer according to element content. The EDX mapping results are shown in Figure 6. As shown in Figure 6a, element Ti was observed in the NTCP specimen. As shown in Figure 6b,c, element Si and element Al were found to be uniformly dispersed within the  $\text{SiO}_2$ - $\text{TiO}_2$  powder and  $\text{Al}_2\text{O}_3$ - $\text{TiO}_2$  powder, respectively. TEM diffraction analysis was performed using Fast Fourier Transform (FFT). As shown in Figures 7 and 8, the results confirmed that  $\text{SiO}_2$  and  $\text{Al}_2\text{O}_3$  were the core materials of the NTCP. Additionally, the shell part was determined to be anatase  $\text{TiO}_2$  phase.



**Figure 6.** Mapping image of NTCP (a) Ti (b) Si (c) Al.



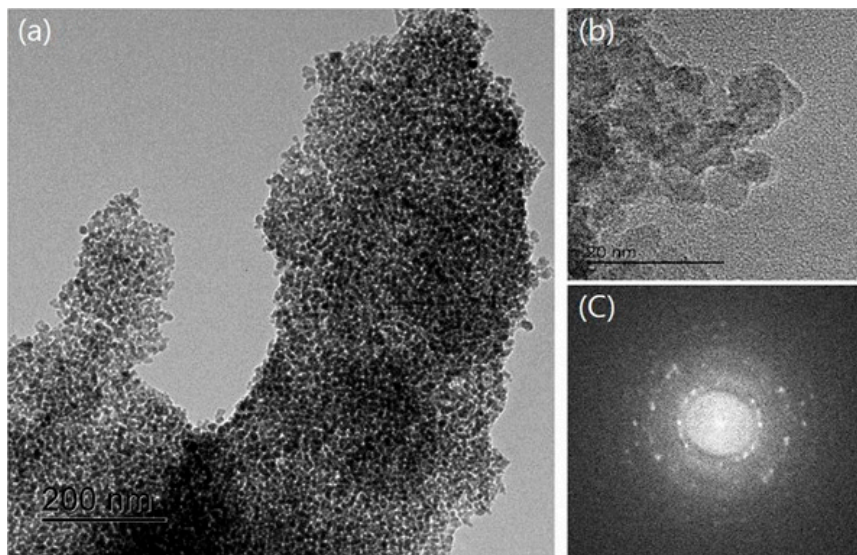


**Figure 7.** TEM image of  $\text{Al}_2\text{O}_3\text{-TiO}_2$  (a) TEM photo. (b) Magnifying TEM photo and (c) its fast Fourier transform (FFT) pattern.

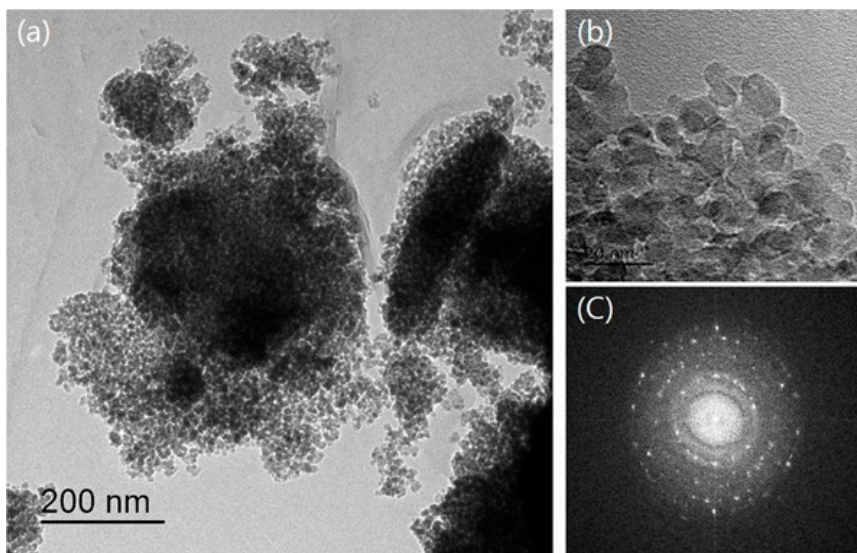


**Figure 8.** TEM image of  $\text{SiO}_2\text{-TiO}_2$  (a) TEM photo. (b) Magnifying TEM photo and (c) its fast Fourier transform (FFT) pattern.

### 3.5. UV-VIS Analysis

UV fluorescence analysis was conducted on both commercial  $\text{TiO}_2$  and the NTCP, and the results are shown in Figure 9. A typical UV light induced photocatalyst is activated at wavelengths of 380 nm or below, triggering a photocatalytic reaction. The results show that the developed NTCP has a light absorption peak at wavelengths of 380 nm or below, and its absorbance is much larger than that of commercial  $\text{TiO}_2$ .

The major findings of the present study confirmed that the developed NTCP is capable of being activated when illuminated by light at wavelengths of 380 nm or below (UV light spectrum) and, thus, will perform as an efficient photocatalyst to decompose  $\text{NO}_x$ .



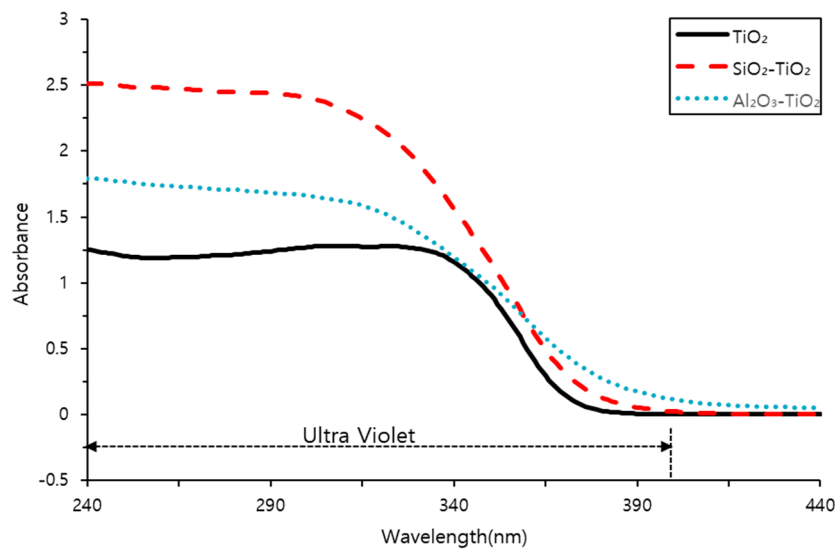


Figure 9. UV-VIS absorbance of commercial  $\text{TiO}_2$  and NTCP.

### 3.6. Flowability of Mortars

The flow ability characteristics of mortar mixed with commercial  $\text{TiO}_2$  and NTCP are shown in Figure 10. The Figure shows the influence of nano powder content on the flowability of mixtures at constant water to binder ratio of 50%. The results show that all the mixes blended with nano powder showed a decline in flow value as the percentage of nano powders increased in the mix. The decrease in the flowability was most evident in  $\text{SiO}_2\text{-TiO}_2$  powder mortar mix.

The reason for this decrease in the flow value is because the specific surface area mixed with mortar and the surface of the nanoparticle with a large volume ratio binds a large number of water molecules, which rapidly reduces free water. In the case of nanoparticles, the larger the specific surface area, the more pronounced the adsorption or other reactions [31,32]. In particular, as the pore size decreases, the potentials in the pores overlap to increase the adsorption strength [33]. As shown in Table 7, the size of the pores of the  $\text{SiO}_2\text{-TiO}_2$  and  $\text{Al}_2\text{O}_3\text{-TiO}_2$  powders used in the mortar mixtures was measured to be 48 Å and 55 Å, respectively, which were smaller than 82 Å of commercial  $\text{TiO}_2$ . Therefore, the flowability decreased by rapidly reducing the free water in the mortar as the surface of the NTCP that has a relatively large specific surface area and volume ratio and stronger adsorption strength than the commercial  $\text{TiO}_2$  binds and adsorbs a large number of water molecules.

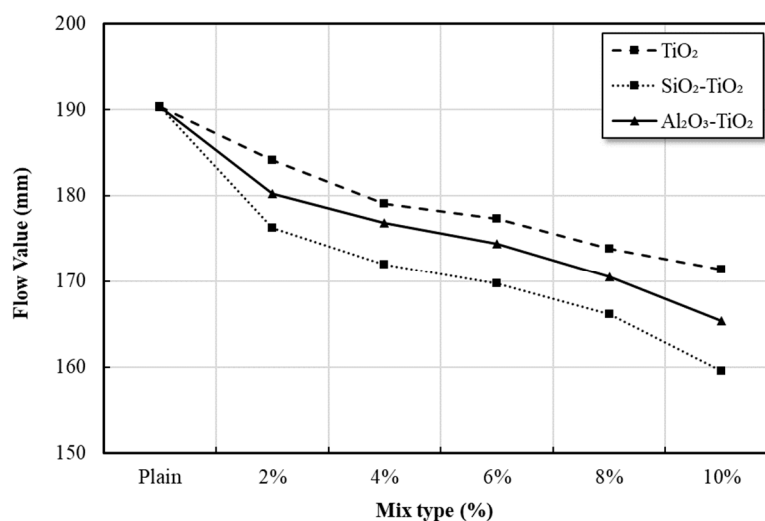


Figure 10. Effects of addition ratio of commercial  $\text{TiO}_2$  and NTCP on cement mortar flow value.

### 3.7. Strengths

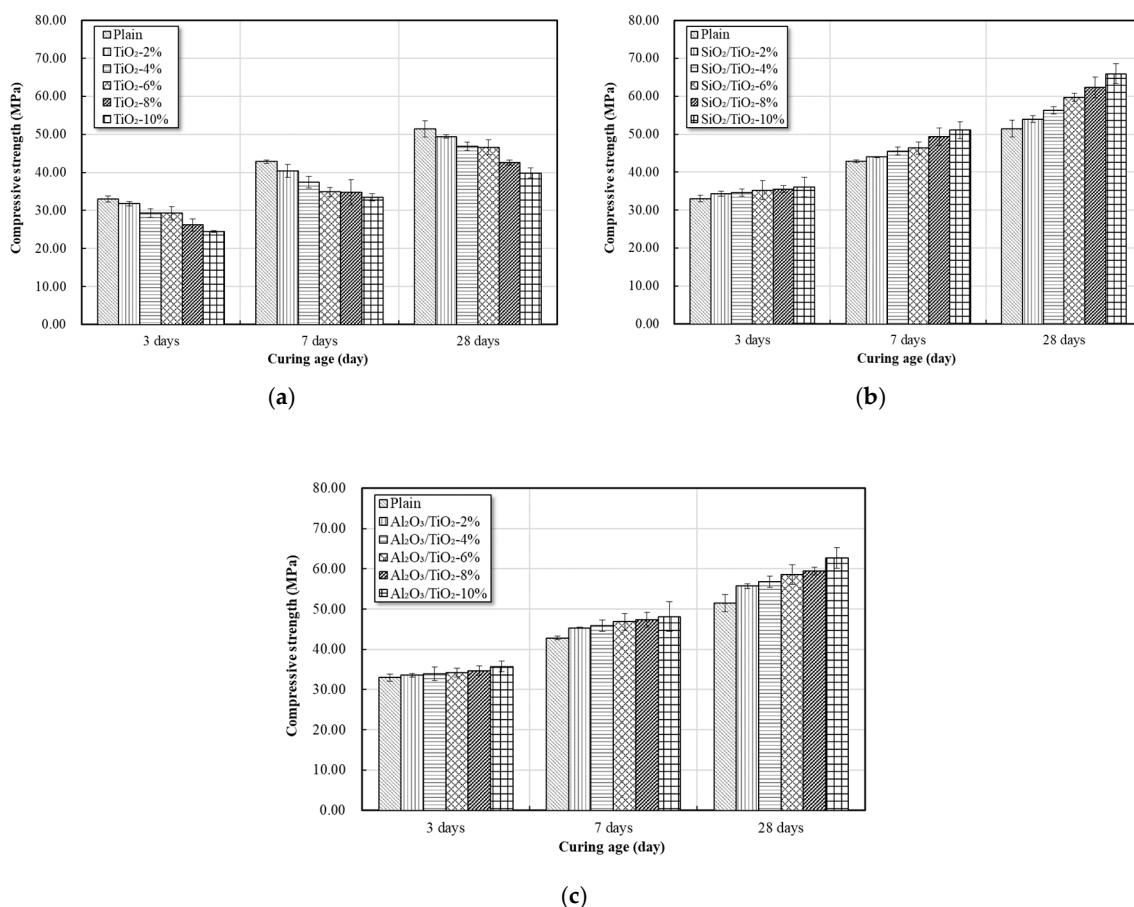
The seven-day, 14-day, and 28-day strengths of mortar produced with partial replacement of each mix (0 to 10%) were measured, as shown in Figures 11 and 12.

As the replacement ratio of commercial  $\text{TiO}_2$  increased, a decrease in the compressive strength was observed, and the compressive strength increased according to the replacement ratio of the NTCP. In all mixes, the compressive strength tended to increase as the curing age increased.

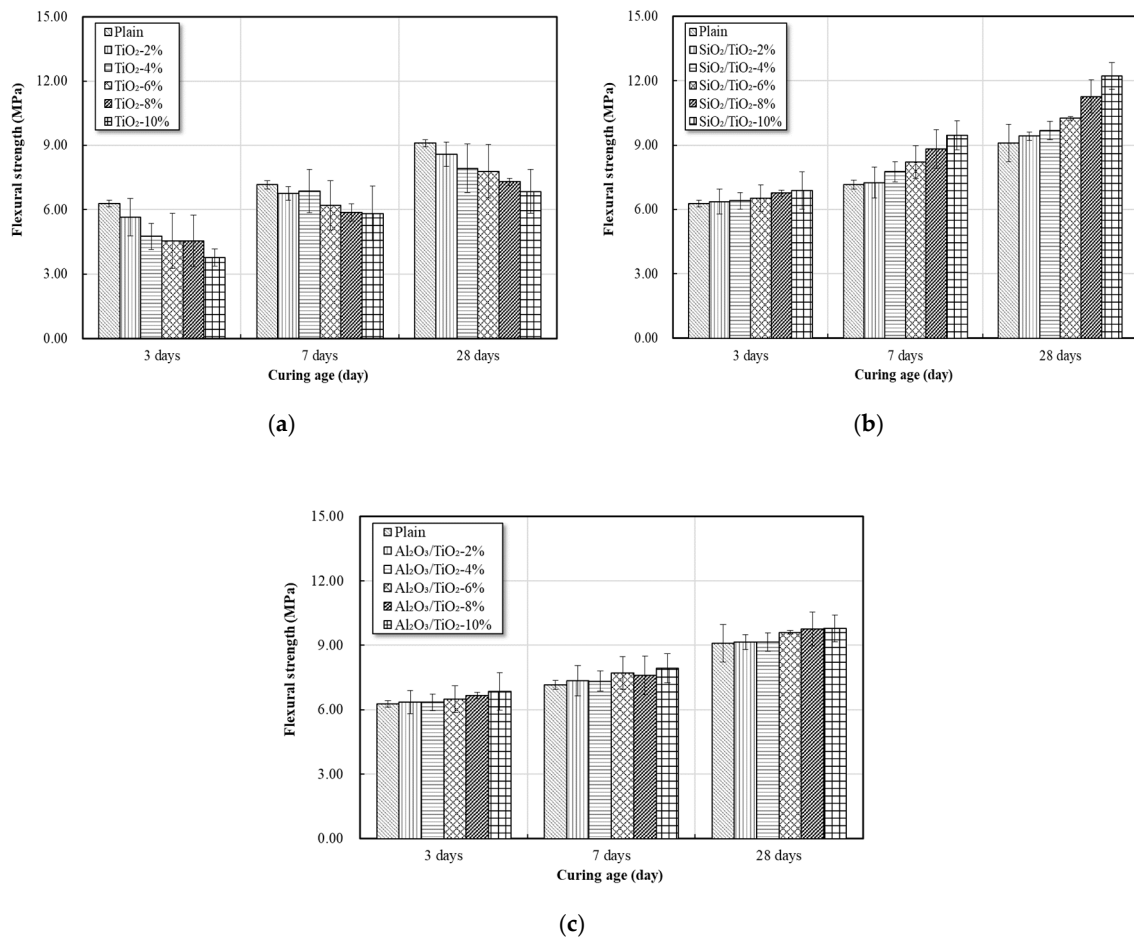
In the case of replacing commercial  $\text{TiO}_2$  at the early curing age of three days, the compressive strength decreased by 3.6–25.8% compared to plain, and the compressive strength increased up to 9.3% when replacing  $\text{SiO}_2$ - $\text{TiO}_2$  powder and up to 8.3% when replacing  $\text{Al}_2\text{O}_3$ - $\text{TiO}_2$  powder.

At the curing age of seven days, in the case of replacing commercial  $\text{TiO}_2$ , the compressive strength decreased as the replacement ratio increased, showing a decrease in strength by 5.7–21.8% compared to plain. In the case of using  $\text{SiO}_2$ - $\text{TiO}_2$  powder, the compressive strength increased by 2.7–19.2% as the replacement ratio increased. The compressive strength also increased by 5.8–12.4% when using  $\text{Al}_2\text{O}_3$ - $\text{TiO}_2$  powder.

At the curing age of 28 days, the compressive strength decreased by 3.9–22.6% in the case of replacing commercial  $\text{TiO}_2$ , and similar to the results of the third and seventh days, the compressive strength decreased as the replacement ratio increased. In the case of using  $\text{SiO}_2$ - $\text{TiO}_2$  powder, the compressive strength increased by 4.8–28% as the replacement ratio increased. The compressive strength also increased by 8.3–21.7% when using  $\text{Al}_2\text{O}_3$ - $\text{TiO}_2$  powder. The flexural strength of each mix was similar to that of the compressive strength. The compressive strength and flexural strength decreased as the amount of replaced commercial  $\text{TiO}_2$  increased [34].

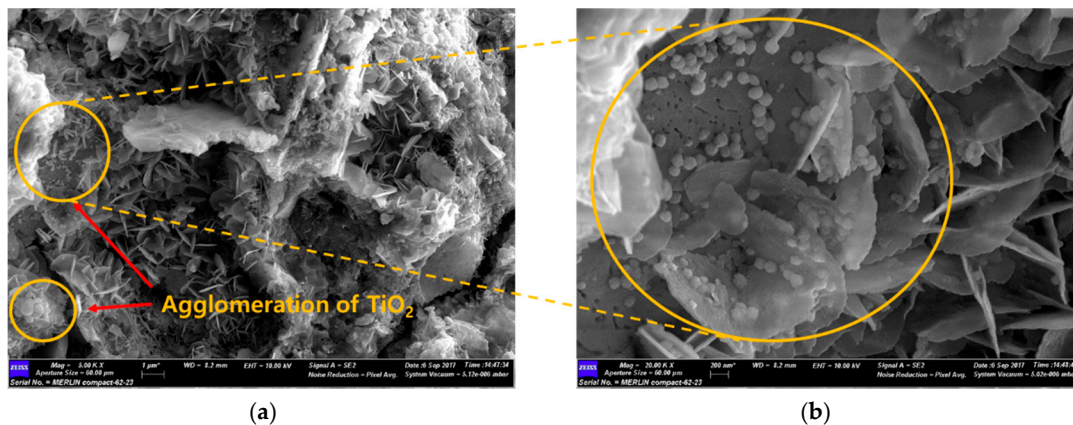


**Figure 11.** Effects of addition ratio of nano powder on compressive strength, (a) commercial  $\text{TiO}_2$ ; (b)  $\text{SiO}_2$ - $\text{TiO}_2$  powder; and (c)  $\text{Al}_2\text{O}_3$ - $\text{TiO}_2$  powder.



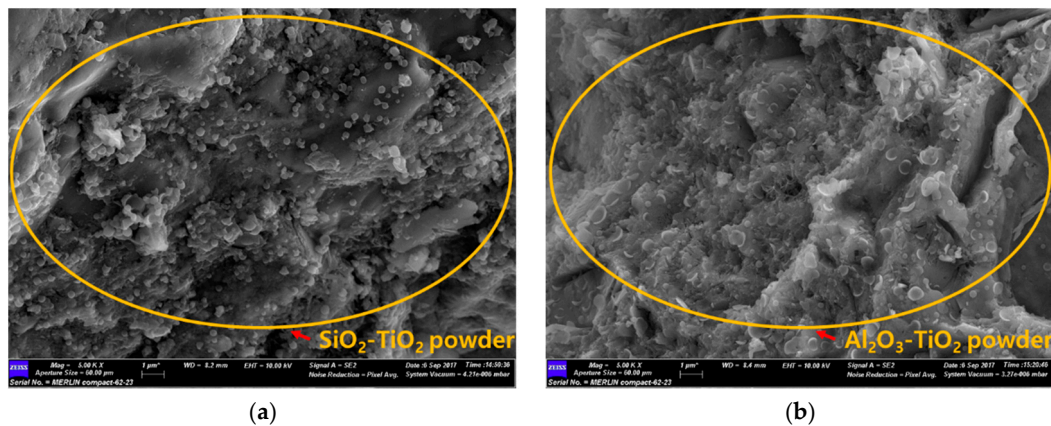
**Figure 12.** Effects of addition ratio of nano powder on flexural strength, (a) commercial TiO<sub>2</sub>; (b) SiO<sub>2</sub>-TiO<sub>2</sub> powder; and (c) Al<sub>2</sub>O<sub>3</sub>-TiO<sub>2</sub> powder.

Figure 13 is a SEM image of mortar mixed with commercial TiO<sub>2</sub>. It is considered that commercial TiO<sub>2</sub> is not uniformly distributed within the cement matrix, but exists in a concentrated form in the hydrate, which interferes with the hydration reaction of the cement and, therefore, the strength development is not achieved. In particular, as the mixing amount of commercial TiO<sub>2</sub> increases, the size and number of aggregates increase, which is likely to contribute as stress raisers that reduce the strength of mortar [35].



**Figure 13.** SEM image of mortar mixed with commercial TiO<sub>2</sub> at day 3. (a) Agglomeration of TiO<sub>2</sub> (5000×); and (b) agglomeration of TiO<sub>2</sub> (20,000×).

On the other hand, when replacing  $\text{SiO}_2\text{-TiO}_2$  powder and  $\text{Al}_2\text{O}_3\text{-TiO}_2$  powder, the flexural strength and compressive strength tended to increase as the amount of replacement increased. Unlike commercial  $\text{TiO}_2$ , the NTCP is uniformly dispersed within the cement matrix as shown in Figure 14. This is because the NTCP modified by  $\text{SiO}_2$  and  $\text{Al}_2\text{O}_3$  used as support materials produces Ti-O-Si and Ti-O-Al bond and generates more negative charges that can be dispersed in the matrix.



**Figure 14.** SEM image of mortar mixed with NTCP at day 3. (a)  $\text{SiO}_2\text{-TiO}_2$  powder (5000 $\times$ ); and (b)  $\text{Al}_2\text{O}_3\text{-TiO}_2$  powder (5000 $\times$ )

In addition, the influence of the NTCP in the matrix can be determined by the  $\text{Ca(OH)}_2$  (CH) orientation. The CH orientation can be calculated according to the calculation given in [34]. After obtaining the CH (001) and (101) crystal face peak intensities through XRD, it is defined by the orientation index  $R$  according to the following Equation (1):

$$R = 1.35 I_{(001)} / I_{(101)} \quad (1)$$

where  $I_{(001)}$  and  $I_{(101)}$  are the (001) and (101) crystal face peak intensities, respectively. The results are shown in Table 8. The orientation index of CH decreased when the NTCP was mixed. At day 1, the indices of CH in OPC,  $\text{TiO}_2$ ,  $\text{SiO}_2\text{-TiO}_2$ , and  $\text{Al}_2\text{O}_3\text{-TiO}_2$  are 3.7, 2.7, 2.1, and 2.3, respectively. At day 7, the indices of CH in OPC,  $\text{TiO}_2$ ,  $\text{SiO}_2\text{-TiO}_2$ , and  $\text{Al}_2\text{O}_3\text{-TiO}_2$  are 3.6, 3.5, 1.8, and 1.9, respectively. The results reveal that NTCP can decrease the orientation of CH crystals in matrix.

This is due to the pozzolanic reaction between  $\text{SiO}_2$ ,  $\text{Al}_2\text{O}_3$ , and CH used as support materials. This reaction consumes some of the CH, promotes the hydration reaction, and can generate more calcium silicate hydrate (C-S-H) and calcium aluminate hydrate (C-A-H) [36,37].

**Table 8.** Diffraction intensity and orientation of CH at curing ages of one day and seven days.

Powder	1 Day			7 Day		
	(001) CH	(101) CH	CH Orientation	(001) CH	(101) CH	CH Orientation
OPC	409	150	3.7 ( $\pm 0.2$ )	478	178	3.6 ( $\pm 0.1$ )
$\text{TiO}_2$	288	144	2.7 ( $\pm 0.3$ )	396	154	3.5 ( $\pm 0.2$ )
$\text{SiO}_2\text{-TiO}_2$	310	196	2.1 ( $\pm 0.1$ )	230	171	1.8 ( $\pm 0.1$ )
$\text{Al}_2\text{O}_3\text{-TiO}_2$	304	182	2.3 ( $\pm 0.4$ )	269	182	1.9 ( $\pm 0.2$ )

As shown in Figure 15, the C-S-H and C-A-H formed by the pozzolanic reaction attach to the surface of the NTCP and promote a nucleation effect. Therefore, the CH crystals in the mortar can be refined to reduce the negative impact on the matrix strength by CH. In addition, the strength of mortar is considered to be improved because the matrix is smaller which increases the density to reduce the filling effect and the number of harmful holes [38].



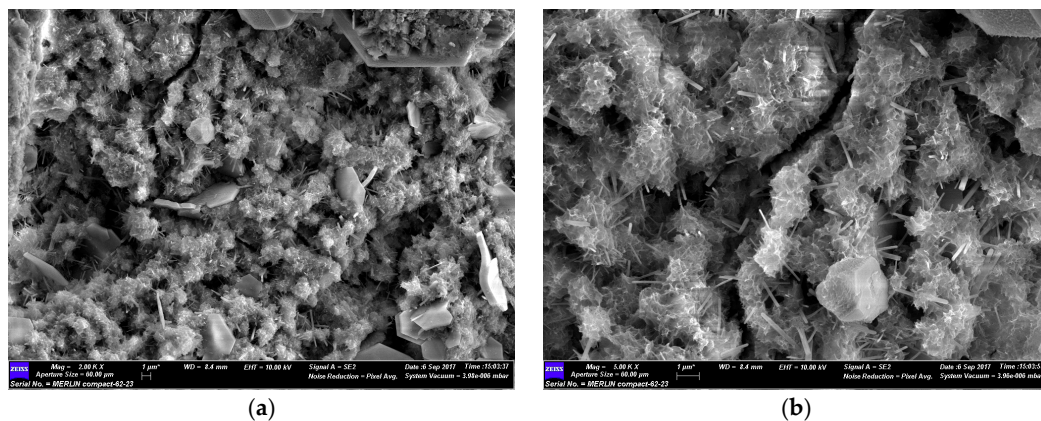


**Figure 15.** SEM image of nucleation effect by NTCP at day 3. (a) NTCP (2000 $\times$ ); and (b) NTCP (5000 $\times$ ).

#### 4. Conclusions

The purpose of this study is to increase the use of  $\text{TiO}_2$  as a construction material as part of the research to purify air pollution. To that end, NTCP was synthesized by coating  $\text{SiO}_2$  and  $\text{Al}_2\text{O}_3$  support materials with  $\text{TiO}_2$ . Subsequently, the developed NTCP and commercial  $\text{TiO}_2$  were analyzed and compared. Major findings of the present study are as follows:

- (1) XRD, SEM, and TEM analyses confirmed that the NTCP developed in the present study was anatase phase spherical particles. Its particles were smaller and more uniform in size than the commercial  $\text{TiO}_2$ , and the average particle size of the  $\text{SiO}_2$ - $\text{TiO}_2$  powder and  $\text{Al}_2\text{O}_3$ - $\text{TiO}_2$  powder was 8.36 nm and 9.42 nm, respectively. UV absorption test results showed the developed NTCP had a light absorption peak at wavelengths of 380 nm or below, and its absorbance was much larger than that of commercial  $\text{TiO}_2$ .
- (2) As a result of the flow test, the flow value decreased as the replacement ratio of the NTCP increased. The reason for this decrease in the flow value is because the adsorption strength increased and combined a large number of water molecules, indicating that it is necessary to use a proper admixture according to each mix.
- (3) As a result of the strength test, the pozzolanic reaction by  $\text{SiO}_2$  and  $\text{Al}_2\text{O}_3$  used as support materials produced many C-S-H and C-A-H. In addition, NTCP has shown an increased strength to that of plain and commercial  $\text{TiO}_2$  mortar by promoting a nucleation effect and reducing the filling effect and the number of harmful holes in the mortar.
- (4) This study fabricated a NTCP and evaluated the performance, and the results showed that the performance was equal to or better than the existing products when applied to mortar. In addition to quantitative studies on pozzolanic reactions within the mortar matrix that applies NTCP, evaluation test on  $\text{NO}_x$  removal performance should also be conducted for use on site.

**Author Contributions:** Methodology: J.-W.L. and Y.-I.J.; experiment: J.-W.L. and Y.-I.J.; validation: Y.-I.J.; formal analysis: J.-W.L., Y.-I.J., and B.-J.L.; investigation: J.-W.L. and Y.-I.J.; data curation: J.-W.L. and Y.-I.J.; writing—original draft preparation: J.-W.L., Y.-I.J., and B.-J.L.; writing—review and editing: S.-W.K., W.-S.P., B.-J.L., and Y.-I.J.; visualization: J.-W.L. and B.-J.L.; supervision: S.-W.K., W.-S.P., and Y.-I.J.; project administration: Y.-I.J.

**Funding:** This research was supported by Basic Science Research Program through the National Research Foundation of Korea (NRF) funded by the Ministry of Education (no. 2015R1D1A1A01058109 and 2018R1D1A1A09082743).

**Conflicts of Interest:** The authors declare no conflict of interest.



## References

1. Kan, H.; London, S.J.; Chen, G.; Zhang, Y.; Song, G.; Zhao, N.; Jiang, L.; Chen, B. Season, sex, age, and education as modifiers of the effects of outdoor air pollution on daily mortality in Shanghai, China: The Public Health and Air Pollution in Asia (PAPA) study. *Environ. Health Perspect.* **2008**, *116*, 1183–1188. [CrossRef]
2. Chen, B.; Hong, C.; Kan, H. Exposures and health outcomes from outdoor air pollutants in China. *Toxicology* **2004**, *198*, 291–300. [CrossRef]
3. Hong, S.J.; Lee, S.W. An Experimental Study for the Construction of Photocatalytic Method Concrete Road Structure. *J. Korean Soc. Road Eng.* **2013**, *15*, 1–9. [CrossRef]
4. Fujishima, A.; Rao, T.N.; Tryk, D.A. Titanium dioxide photocatalysis. *J. Photochem. Photobiol. C Photochem. Rev.* **2017**, *1*, 5525. [CrossRef]
5. Henderson, M.A. A surface science perspective on TiO<sub>2</sub> photocatalysis. *Surf. Sci. Rep.* **2011**, *66*, 185–297. [CrossRef]
6. Guo, M.-Z.; Ling, T.-C.; Poon, C.-S. TiO<sub>2</sub>-based self-compacting glass mortar: Comparison of photocatalytic nitrogen oxide removal and bacteria inactivation. *Build. Environ.* **2012**, *53*, 1–6. [CrossRef]
7. Guo, M.-Z.; Ling, T.-C.; Poon, C.-S. Nano-TiO<sub>2</sub>-based architectural mortar for NO removal and bacteria inactivation: Influence of coating and weathering conditions. *Cem. Concr. Compos.* **2013**, *36*, 101–108. [CrossRef]
8. Jameel, Z.N.; Haider, A.J.; Taha, S.Y.; Gangopadhyay, S.; Bok, S. Evaluation of hybrid sol-gel incorporated with nanoparticles as nano paint. In *AIP Conference Proceedings*; AIP Publishing: Beirut, Lebanon, 2016; Volume 1758, p. 020001.
9. Haider, A.J.; Materials, A.; Materials, A. Synthesis and Characterization of TiO<sub>2</sub> Nanoparticles via Sol-Gel Method by Pulse Laser Ablation. *Eng. Technol. J.* **2015**, *33*, 761–771.
10. Sirimahachai, U.; Phongpaichit, S.; Wongnawa, S. Evaluation of bactericidal activity of TiO<sub>2</sub> photocatalysts: A comparative study of laboratory-made and commercial TiO<sub>2</sub> samples. *Songklanakarin J. Sci. Technol.* **2009**, *31*, 517–525.
11. Qi, M.; Yang, D.; Zhang, J.; Forum, H.A.-M.S. Undefined Preparation and Characterization of Zn-Containing Hydroxyapatite/TiO<sub>2</sub> Composite Coatings on Ti Alloys. *Trans. Tech. Publ.* **2011**, *685*, 367–370.
12. Balbuena, J.; Sánchez, L.; Cruz-Yusta, M. Use of Steel Industry Wastes for the Preparation of Self-Cleaning Mortars. *Materials* **2019**, *12*, 621. [CrossRef] [PubMed]
13. Poon, C.S.; Cheung, E. NO removal efficiency of photocatalytic paving blocks prepared with recycled materials. *Constr. Build. Mater.* **2007**, *21*, 1746–1753. [CrossRef]
14. Chen, J.; Poon, C. Photocatalytic construction and building materials: From fundamentals to applications. *Build. Environ.* **2009**, *44*, 1899–1906. [CrossRef]
15. Chen, J.; Poon, C.S. Photocatalytic activity of titanium dioxide modified concrete materials—Influence of utilizing recycled glass cullets as aggregates. *J. Environ. Manag.* **2009**, *90*, 3436–3442. [CrossRef]
16. Guo, M.Z.; Poon, C.S. Photocatalytic NO removal of concrete surface layers intermixed with TiO<sub>2</sub>. *Build. Environ.* **2013**, *70*, 102–109. [CrossRef]
17. Beeldens, A. An environmental friendly solution for air purification and self-cleaning effect: the application of TiO<sub>2</sub> as photocatalyst in concrete. In *Proceedings of the Transport Research Arena Europe–TRA, Göteborg, Sweden, 12–16 June 2006*.
18. Available online: [http://www.italcementigroup.com/NR/rdonlyres/B5F973F4-8D01-4796-ACEC-1A960C71092E/0/QA\\_UK.Pdf](http://www.italcementigroup.com/NR/rdonlyres/B5F973F4-8D01-4796-ACEC-1A960C71092E/0/QA_UK.Pdf) (accessed on 18 January 2019).
19. Verdier, T.; Coutand, M.; Bertron, A.; Roques, C. Antibacterial activity of TiO<sub>2</sub> photocatalyst alone or in coatings on E. coli: The influence of methodological aspects. *Coatings* **2014**, *4*, 670–686. [CrossRef]
20. Ba-Abbad, M.M.; Kadhum, A.A.H.; Mohamad, A.B.; Takriff, M.S.; Sopian, K. Synthesis and catalytic activity of TiO<sub>2</sub> nanoparticles for photochemical oxidation of concentrated chlorophenols under direct solar radiation. *Int. J. Electrochem. Sci.* **2012**, *7*, 4871–4888.
21. Kim, Y.K.; Hong, S.J.; Lee, K.B.; Lee, S.W. Evaluation of NO<sub>x</sub> Removal Efficiency of Photocatalytic Concrete for Road Structure. *J. Korean Soc. Road Eng.* **2014**, *16*, 49–58. [CrossRef]
22. Murata, Y.; Kamitani, K.; Takeuchi, K. Air purifying blocks based on photocatalysis. In *Proceedings of the Japan Interlocking Block Pavement Engineering Association World Congress, Tokyo, Japan, 16–19 July 2000*.

23. Guo, M.-Z.; Ling, T.-C.; Poon, C.S. Photocatalytic NO<sub>x</sub> degradation of concrete surface layers intermixed and spray-coated with nano-TiO<sub>2</sub>: Influence of experimental factors. *Cem. Concr. Compos.* **2017**, *83*, 279–289. [[CrossRef](#)]
24. Han, B.; Li, Z.; Zhang, L.; Zeng, S.; Yu, X.; Han, B.; Ou, J. Reactive powder concrete reinforced with nano SiO<sub>2</sub>-coated TiO<sub>2</sub>. *Constr. Build. Mater.* **2017**, *148*, 104–112. [[CrossRef](#)]
25. Kamaruddin, S.; Stephan, D. Sol-gel mediated coating and characterization of photocatalytic sand and fumed silica for environmental remediation. *Water Air Soil Pollut.* **2014**, *225*, 1948. [[CrossRef](#)]
26. Park, O.K.; Kang, Y.S.; Jo, B.G. Synthesis of TiO<sub>2</sub> nanoparticles coated with SiO<sub>2</sub> for suppression of photocatalytic activity and increased dispersion stability. *J. Industr. Eng. Chem.* **2004**, *10*, 733–738.
27. Liu, Y.L.; Cao, C.C.; Chen, J. Preparation of Photocatalyst of Nano-TiO<sub>2</sub> Coating on SiO<sub>2</sub> carriers and its Photocatalytic Activity. *Adv. Mater. Res.* **2013**, *777*, 77–81. [[CrossRef](#)]
28. Rossi, E.M.; Pylkkänen, L.; Koivisto, A.J.; Vippola, M.; Jensen, K.A.; Miettinen, M.; Sirola, K.; Nykäsenoja, H.; Karisola, P.; Stjernvall, T.; et al. Airway Exposure to Silica-Coated TiO<sub>2</sub> Nanoparticles Induces Pulmonary Neutrophilia in Mice. *Toxicol. Sci.* **2010**, *113*, 422–433. [[CrossRef](#)] [[PubMed](#)]
29. Vohra, M.S.; Tanaka, K. Photocatalytic degradation of aqueous pollutants using silica-modified TiO<sub>2</sub>. *Water Res.* **2003**, *37*, 3992–3996. [[CrossRef](#)]
30. Yuranova, T.; Sarria, V.; Jardim, W.; Rengifo, J.; Pulgarin, C.; Trabesinger, G.; Kiwi, J. Photocatalytic discoloration of organic compounds on outdoor building cement panels modified by photoactive coatings. *J. Photochem. Photobiol. A Chem.* **2007**, *188*, 334–341. [[CrossRef](#)]
31. Alivisatos, A.P. Semiconductor Clusters, Nanocrystals, and Quantum Dots. *Science* **1996**, *271*, 933–937. [[CrossRef](#)]
32. Vepřek, S. Electronic and mechanical properties of nanocrystalline composites when approaching molecular size. *Thin Solid Films* **1997**, *297*, 145–153. [[CrossRef](#)]
33. Park, J.W.; Oh, H.C. Development of a Cost-Effective 20K Hydrogen BET Measurement for Nanoporous Materials. *Korean J. Mater. Res.* **2017**, *27*, 466–470. [[CrossRef](#)]
34. Cerro-Prada, E.; García-Salgado, S.; Quijano, M.; Varela, F. Controlled Synthesis and Microstructural Properties of Sol-Gel TiO<sub>2</sub> Nanoparticles for Photocatalytic Cement Composites. *Nanomaterials* **2019**, *9*, 26. [[CrossRef](#)]
35. Collins, F.; Lambert, J.; Duan, W.H. The influences of admixtures on the dispersion, workability, and strength of carbon nanotube–OPC paste mixtures. *Cem. Concr. Compos.* **2012**, *34*, 201–207. [[CrossRef](#)]
36. Qing, Y.; Zenan, Z.; Deyu, K.; Rongshen, C. Influence of nano-SiO<sub>2</sub> addition on properties of hardened cement paste as compared with silica fume. *Constr. Build. Mater.* **2007**, *21*, 539–545. [[CrossRef](#)]
37. Meng, T.; Yu, Y.; Qian, X.; Zhan, S.; Qian, K. Effect of nano-TiO<sub>2</sub> on the mechanical properties of cement mortar. *Constr. Build. Mater.* **2012**, *29*, 241–245. [[CrossRef](#)]
38. Qudoos, A.; Kim, H.; Ryou, J.S. Influence of Titanium Dioxide Nanoparticles on the Sulfate Attack upon Ordinary Portland Cement and Slag-Blended Mortars. *Materials* **2018**, *11*, 356. [[CrossRef](#)]

